



Elucidating the links between N₂O dynamics and changes in microbial communities following saltwater intrusions

Rongrong Xie^{a,b,c,*}, Laichang Lin^{a,1}, Chengchun Shi^d, Peng Zhang^e, Peiyuan Rao^a, Jiabing Li^{a,b}, Dandan Izabel-Shen^{f,g,**}

^a College of Environmental and Resource Science, Fujian Normal University, Fuzhou, 350117, China

^b Key Laboratory of Pollution Control and Resource Recycling of Fujian Province, Fujian Normal University, Fuzhou, 350117, China

^c Leibniz Institute for Baltic Sea Research, Warnemünde, Rostock, 18119, Germany

^d Fujian Research Academy of Environmental Sciences, Fuzhou, 350013, China

^e School of Environmental and Municipal Engineering, North China University of Water Resources and Electric Power, Zhengzhou, 450046, China

^f Helmholtz Institute for Functional Marine Biodiversity at the University of Oldenburg (HIFMB), Oldenburg, 26129, Germany

^g Alfred-Wegener-Institute, Helmholtz Centre for Polar and Marine Research, Bremerhaven, 27570, Germany

ARTICLE INFO

Keywords:

Estuary
Greenhouse gases
Denitrification
Microbial community
Nitrogen gene

ABSTRACT

Saltwater intrusion in estuarine ecosystems alters microbial communities as well as biogeochemical cycling processes and has become a worldwide problem. However, the impact of salinity intrusion on the dynamics of nitrous oxide (N₂O) and associated microbial community are understudied. Here, we conducted field microcosms in a tidal estuary during different months (December, April and August) using dialysis bags, and microbes inside the bags encountered a change in salinity in natural setting. We then compared N₂O dynamics in the microcosms with that in natural water. Regardless of incubation environment, saltwater intrusion altered the dissolved N₂O depending on the initial saturation rates of N₂O. While the impact of saltwater intrusion on N₂O dynamics was consistent across months, the dissolved N₂O was higher in summer than in winter. The N-related microbial communities following saltwater intrusion were dominated by denitrifiers, with fewer nitrifiers and bacterial taxa involved in dissimilatory nitrate reduction to ammonium. While denitrification was a significant driver of N₂O dynamics in the studied estuary, nitrifier-involved denitrification contributed to the additional production of N₂O, evidenced by the strong associations with *amoA* genes and the abundance of *Nitrospira*. Higher N₂O concentrations in the field microcosms than in natural water limited N₂O consumption in the former, given the lack of an association with *nosZ* gene abundance. The differences in the N₂O dynamics observed between the microcosms and natural water could be that the latter comprised not only indigenous microbes but also those accompanied with saltwater intrusion, and that immigrants might be functionally rich individuals and able to perform N transformation in multiple pathways. Our work provides the first quantitative assessment of *in situ* N₂O concentrations in an estuary subjected to a saltwater intrusion. The results highlight the importance of ecosystem size and microbial connectivity in the source-sink dynamics of N₂O in changing environments.

1. Introduction

Estuaries are transition zones between rivers and the ocean and hotspots of microbially mediated biogeochemical cycling (Wolanski and Elliott, 2015). However, the riverine transport of anthropogenically-emitted nitrogen in many estuaries has degraded the

water quality. As a result, estuarine waterways have become significant sources of the potent greenhouse gas nitrous oxide (N₂O), with estuarine N₂O emissions accounting for ~18% of global ocean emissions (Bange, 2006; Sierra et al., 2017; Bange et al., 2019). The increased N concentrations in river water due to anthropogenic discharge promote the production of dissolved N₂O (Wells et al., 2018), modulated by the flow

* Corresponding author. Fujian Normal University, Wulongjiang middle Rd. 18, 350117, Fuzhou, China.

** Corresponding author. Helmholtz Institute for Functional Marine Biodiversity at the University of Oldenburg (HIFMB), Ammerländer Heerstraße 231, 26129, Oldenburg, Germany.

E-mail addresses: xierr1118@163.com (R. Xie), dand.shen@gmail.com (D. Izabel-Shen).

¹ The authors contributed equally to this work.

rate and flow variability (Li et al., 2022). Moreover, the frequent saltwater intrusions into estuaries (i.e., saltwater penetrating further up the estuary and salinity there is higher than previously), triggered by rising sea levels (Barlow and Reichard, 2010; Church et al., 2013), could alter dissolved N_2O concentrations (Harley et al., 2015; Xie et al., 2020). However, the effect of saltwater intrusion on dissolved N_2O production and the underlying mechanisms are largely unknown.

N_2O concentration in estuarine water depends on the gas exchange rate and N_2O production, which is influenced by physiochemical properties such as nitrogen concentrations, water temperature and velocity (Li et al., 2022). Nitrogen cycling is also determined to some extent by the concentration of dissolved oxygen (DO), because N_2O is an important intermediate in nitrification under oxygen-rich conditions and in denitrification under oxygen-poor conditions (Bange, 2008; Beaulieu et al., 2011). However, nitrifier denitrification may also occur in oxygen-rich environments, in which plastic particles and suspended particulate matter create an anoxic microsite leading to N_2O production (Zhu et al., 2018; Su et al., 2022). High temperature generally increases N_2O production due to the elevated denitrification rate (Rosamond et al., 2012; Comer-Warner et al., 2023). Conversely, high-velocity currents hinder the biological processes that mediate N_2O production and thus the accumulation of dissolved N_2O (Li et al., 2022; Xia et al., 2017). During saltwater intrusion, all of these physicochemical properties of estuarine systems are significantly altered by the reverse flow, but the coupled effects on dissolved N_2O dynamics are unclear.

The seasonal variation of N_2O in estuarine has gained worldwide attentions (Murray et al., 2015; Wells et al., 2018). The contrasting N_2O dynamics between dry season and wet season were found in three tropical estuaries (Murray et al., 2020). N_2O seasonality was also detected even in different regions of the same estuary. For examples, the N_2O in the upper estuary during winter was higher than that in summer, whereas no significant seasonal difference was exhibited within the middle and lower estuaries (Lin et al., 2016). Hence, the seasonal changes of N_2O and the factors that underlie those changes remain to be further explored.

Within the estuaries, the dominant pathways for N_2O production and thus the major drivers of N_2O sources and sinks are denitrification, followed by nitrification and dissimilatory nitrate reduction to ammonium (DNRA), in the latter N_2O is released as a by-product (Hu et al., 2015; Murray et al. 2015, 2020). Traditional denitrifiers produce N_2O in a stepwise reduction of NO_3^- to N_2 . They can be identified by identifying the genes *nirK*, *nirS* and *norB* (Henry et al., 2006; Kozłowski et al., 2014; Zhao et al., 2018b). N_2O production may also be due to nitrifier denitrification and NH_2OH accumulation by ammonia-oxidizing bacteria (AOB) (Theodorakopoulos et al., 2017). In the nitrifier denitrification pathway of nitrification, ammonia (NH_4^+) is oxidized to nitrite (NO_2^-) followed by the reduction of NH_4^+ , NO_3^- , and NO_2^- to nitric oxide (NO), N_2O , and molecular nitrogen (N_2) (Wrage et al., 2001; Wrage-Mönnig et al., 2018), evidenced by the positive relationship between the abundance of bacterial *amoA* genes and the N_2O content (Ma et al., 2019; Chen et al., 2021b). In addition, both *NIR* and *NOR* genes are crucial for nitrifier denitrification, as demonstrated by Levy-Booth et al. (2014). Ammonia-oxidizing archaea (AOA) also contribute to N_2O production, through a combination of ammonium and nitrite oxidation and the oxidation of intermediated NH_2OH (Santoro et al., 2011; Stieglmeier et al., 2014; Wan et al., 2023). Besides, the complete ammonia oxidation (comammox) has been reported to relate with N_2O production, where a group of microbes convert ammonia into nitrite and then into nitrate through the process of nitrification, such as genus *Nitrospira* (Kits et al., 2019; Han et al., 2021).

Salinity plays an important role in determining the composition of biological communities (Santoro, 2010; Franklin et al., 2017; Wang et al., 2018; Shen et al. 2018a, 2018b). In estuaries, the mixing of freshwater and oceanic water influences their biogeochemistry and microbial activities (Huertas et al., 2018). The very large salinity changes that occur in estuaries between flood tide and ebb tide make

these systems ideal natural laboratories to study the effects of salinity on N_2O production and the underlying drivers of the microbially mediated N cycle. Due to the hydrological conditions of estuarine environments, upstream freshwater is exchanged with sea water twice per day, leading to strong fluctuations in many biogeochemical processes (Cooper et al., 2017). For example, the elevated reactive nitrogen (i.e., NO_3^- , NH_4^+) load from upstream becomes diluted with seawater containing low ambient concentrations of nitrogen, thereby reducing the accumulation of dissolved N_2O , given the ocean water is typically very low in NO_3^- and dissolved N_2O . However, in a previous study conducted under laboratory conditions, i.e., the microbial communities were subjected to salt addition over a period of two months, an increase in salinity promoted N_2O accumulation (Xie et al., 2020). Thus, in estuaries, other confounding effects besides the change in salinity that occurs during saltwater intrusion may influence the behavior of N_2O . In this study, we used field microcosms in which naturally occurring microbes were kept in dialysis bags so that microbes can experience environmental change as those in natural water but did not encounter the immigrant bacteria accompanied with saltwater intrusion. This setup allowed us to disentangle the mechanisms that underlie the previously observed differences in N_2O dynamics in the natural vs. experimental setting. Specifically, we asked: 1) Are there seasonal patterns of dissolved N_2O dynamics? 2) If so, can these patterns be consistently observed in both natural water and the microcosms? 3) To what extent are N_2O dynamics mediated by changes in the microbial community and thus in the relative abundances of nitrogen-related functional genes following saltwater intrusion?

2. Material and methods

2.1. Research area

The Minjiang estuary (119°34'32.4"E, 26°3'2.9"N) (Fig. 1) experiences significant nitrogen contamination, with dissolved total nitrogen (TN) concentrations ranging from 103.29 to 262.42 $\mu\text{mol L}^{-1}$ during saltwater intrusion (Xie et al., 2023). The anthropogenic TN emissions in Fujian city were estimated to be 9257 tons per year (Zhen et al., 2022). This estuary has a typical semi-diurnal tidal regime. The average tidal range in the Minjiang estuary is 4.5 m but it can exceed 6 m (Xie et al., 2017). The Shuikou Dam is located approximately 120 km upstream of the research area and releases a minimum flow of 308 $\text{m}^3 \text{s}^{-1}$ (Xie et al., 2017). Considering those empirical data, the Minjiang estuary provides an ideal system for the study of N_2O dynamics.

2.2. Setup of field microcosms

Field microcosms were established in December 2020 and in April and August 2021, together representing a period of ebb-flood tide and thus the typical hydrological changes (data shown in Table S1). In the experiment, the use of dialysis bags with a molecular mass cutoff of 12–14 kDa (Spectrum Laboratories, CA, United States) ensured the free exchange of dissolved organic matter (DOM) and nutrients while preventing the passage of microorganisms (protists, bacteria and viruses). The dialysis bags allowed the efficient diffusion of most organic molecules because the molecular mass of DOM in aquatic environments is normally <5 kDa (Shen et al., 2018a; Nebbioso and Piccolo, 2013). In order to estimate the lag effect of a salinity equilibrium inside the dialysis bags, the exchange efficiency of water to dialysis bags during salinity intrusion was calculated according to the well-established concepts of conservative mixing as follows:

$$\alpha V S'_{i+1} \Delta t + (V - \alpha V \Delta t) S_i = V S_{i+1} \quad (1)$$

where, α is the exchange efficiency of water to dialysis bag, V is the water volume in dialysis bags, S'_{i+1} is the salinity in NW at $(i+1)^{\text{th}}$ sampling time, Δt is the time interval between i and $i+1$, S_i and S_{i+1} are the salinity in EG at i^{th} and $(i+1)^{\text{th}}$ sampling time, respectively. The

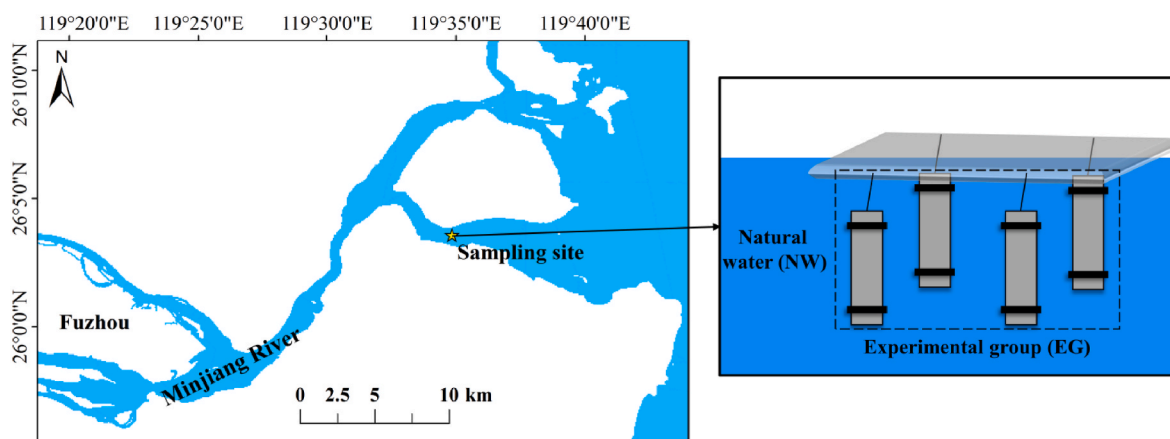


Fig. 1. Map of the surveyed sampling sites and the setup of the field microcosms using dialysis bags. The inset shows the location of the river in southeastern China.

dialysis bag (45 cm long) was rinsed thoroughly for 12 h, soaked in Milli-Q water overnight, and then soaked for another 12 h in fresh Milli-Q water to keep it sterile before use. Twelve h before the setup of the experiment, water was collected from the sampling site, and 1.1 L was subsequently transferred to the dialysis tubing. This sample served as the experimental (microcosm) group (EG). The dialysis bags were deployed at approximately 6:00 am (~12 h after sampling) to ensure that the experiment started under similar hydrodynamic conditions as the water collection. Six to seven timepoints were chosen to achieve high-resolution sampling within a day (Supplementary Table S1). Each treatment consisted of duplicate microcosms for each timepoint, resulting in a total of 12 units in December 2020 and August 2021, and 14 units in April 2021. All dialysis bags were incubated 0.2 m below the surface water in the field, with varying water depths ranging from 0.92 m to 5.33 m during the three months (Supplementary Table S1). In addition to the EG microcosms, at each sampling timepoint natural water (NW), i.e., the surrounding water in which the dialysis bags were incubated, was sampled to serve as a control where microbes were not limited to dispersal and thus could interact with the immigrant bacteria accompanied with saltwater. EG and NW were first sampled after 1 h of incubation (i.e., approximately 7 a.m.) and then at 1.25- to 2.17-h intervals thereafter according to the discharge changes during ebb and flood conditions (Supplementary Table S1). The incubations were carried out for less than a day, hence the formation of biofilm on the surfaces of the bags were rather limited so that the permeability of the dialysis bags was maintained as much as possible during the experiment. Supplementary Table S2 provides an overview of the sampling done for sample processing over time in three different months.

2.3. Environmental context data collection

Salinity and temperature were monitored in the field using a salinometer (CT-3081, Kedida, China). The practical salinity scale was used in this manuscript according to the UNESCO (UNESCO, 1985) definition and it is unitless. DO and pH were measured using a DO meter (HI9147, Hanna, Italy) and a pH meter (RPB10, Haiheng, China), respectively. Turbidity was measured using a turbidimeter (2100Q, HACH, America) and recorded as nephelometric turbidity units. Discharge was measured using a vessel-mounted Acoustic Doppler Current Profiler (RiverRay ADCP, Teledyne RDI, USA) according to the acoustic Doppler backscatter (Woodward and Appell, 1986). The water level was obtained by querying Guantou, a nearby site, via the website of the China Ocean Information Center (www.cnss.com.cn/tide/).

At each time point, the dialysis bags were immediately transported to the laboratory at the *in situ* temperature and destructively sampled for N speciation analysis and the quantification of N-involved functional genes. One liter of water from each dialysis bag and from the NW was

immediately filtered through 0.22- μ m-pore-size filter (Millipore, Darmstadt, Germany) and immediately flash frozen in liquid nitrogen. The samples were stored at -80°C until nucleic acid extraction. The filtrate was kept at 4°C prior to the determination of dissolved inorganic N (NH_4^+ , NO_3^- , and NO_2^-). A standard spectrophotometer (UV-1100, Mapada Instruments, China) was used to measure the concentration of those N compounds as described in our previous work (Xie et al., 2020). A summary of the environmental context data, including the hydrological characteristics and physiochemical parameters of the water, is provided in Supplementary Table S3.

2.4. Dissolved N_2O measurement

Bubble-free water (30 mL) was sampled from all EG and NW and sealed in headspace bottles that were flushed 2–3 times with the sampled water thoroughly prior to filling. Approximately 0.2 mL of saturated HgCl_2 solution was injected into each sample bottle to inhibit microbial activity (Zhang et al., 2013). All the samples were stored at -4°C and analyzed within 24 h after sampling. The dissolved N_2O was measured using the headspace equilibrium technique (Li et al., 2022; Wanninkhof, 1992). Briefly, 10 mL of high-purity nitrogen gas was syringe-injected into the headspace bottle to displace the water sample. After creation of the headspace, the bottle was shaken for 30 min and then placed in the dark for 30 min to allow the N_2O to reach equilibrium between the water and gas phases. The concentration of N_2O in the headspace gas was measured using a gas chromatograph (GC-2014, Shimadzu, Japan) equipped with an electron capture detector. The calculation of the dissolved N_2O concentrations and N_2O saturation was detailed in the Supplementary Text.

2.5. DNA extraction and quantification of functional genes by quantitative polymerase chain reaction (qPCR)

Microbial community characterization and functional gene quantification were restricted to samples taken during the saltwater intrusion period. Genomic DNA from a total of 24 samples was extracted using the TIANamp soil DNA kit (Tiangen Biotech, Beijing) according to the manufacturer's instructions and purified using the TIANamp genomic DNA kit. The concentration and purity of the extracted DNA were determined by gel electrophoresis and Nanodrop 2000 spectrophotometry (Thermo Fisher Scientific, DE, USA). The extracted DNA was stored at -80°C until further processing.

The abundances of the main functional genes involved in nitrification (*amoA*-AOA, *amoA*-AOB, and *nrrA*), denitrification (*nirK*, *nirS*, and *nosZ*), and DNRA (*nrfA*) were quantified (for the primer sequences, see Supplementary Table S2) to test the impact of saltwater intrusion and the resulting microbial dispersal. The genes were quantified by qPCR

using the primers listed in [Supplementary Table S4](#). The 50- μ L PCR volume consisted of 25 μ L $2 \times$ Taq Master Mix, 1 μ L template DNA, 22 μ L sterile water, and 1 μ L each of forward and reverse primers (10 μ M). PCR amplification was carried out using three replicates per sample under the following conditions: initial denaturation at 94 $^{\circ}$ C for 5 min, followed by 30 cycles for 30 s at 94 $^{\circ}$ C, 55 $^{\circ}$ C for 30 s, extension for 30 s at 72 $^{\circ}$ C and a final extension at 72 $^{\circ}$ C for 10 min. A qPCR standard curve was constructed by diluting standard plasmid samples to generate a series of 10-fold dilutions. The threshold cycle (Ct) values were then determined to quantify the copy number of the targeted genes. In this study, the R^2 values of the standard curve were all >0.98 , and the amplification efficiency of the PCR was $>90\%$.

2.6. Microbial community characterization

The composition of the total bacterial community in the EG and in NW was characterized using the 16S rRNA gene (for the primer sequences, see [Table S4](#)). The purified library products were paired-end sequenced on the Illumina Miseq PE300 platform. The sequences were subjected to quality control processing using Trimmomatic (v0.36) (Bolger et al., 2014) and Pear (v0.9.6) (Zhang et al., 2014) to obtain high-quality sequences, which were bioinformatically processed using QIIME, version 1.8.0. A finer resolution was enabled by further denoising the quality trimmed sequences using the UNOISE3 pipeline to generate zero-radius OTUs defined at 100% sequence identity (zOTUs), and then aligning the obtained sequences against the bacterial reference database SILVA v138. Sequences that did not align with the correct region were eliminated. Because the samples of the three months were sequenced separately, the quality-trimmed reads datasets were sub-sampled to 25,926 for December, 30,527 for April, and 28,974 August datasets to standardize the uneven sequencing efforts.

2.7. Statistical analysis

A Wilcoxon signed-rank test was used to assess differences in the concentrations of N contents (NH_4^+ , NO_3^- , and NO_2^-) and dissolved N_2O before and during saltwater intrusion, the differences in the abundance of nitrogen functional genes, and the differences in genus-level bacteria related to nitrogen cycle between the NW and EG. A Kruskal-Wallis test was performed to examine the difference in the relative abundance of N functional genes within NW and EG. A post-hoc test (the Dunn's Test) was used to identify significant comparison pairs and their level of significance, a Bonferroni correction to adjust the p value determined in the paired comparison test. A Pearson correlation analysis to assess the correlation between dissolved N_2O concentrations and physicochemical variables. A linear regression analysis was used to test the relationship between dissolved N_2O concentrations and the absolute abundance of functional genes. A non-metric multidimensional scaling (NMDS) analysis was conducted to visualize the bacterial β -diversity based on the Bray-Curtis distances, and an analysis of similarities (ANOSIM) to test the effects of months and treatments on the bacterial communities. Euclidean clustering of genus-level bacteria was performed as well. All statistical analyses were conducted with IBM SPSS 22.0, and data were visualized using Origin 2021.

3. Results

3.1. Changes in physicochemical properties of estuarine water following saltwater intrusion

In December 2020, April 2021, and August 2021, the salinity was similar during each of the first two sampling timepoints but it then started to rise at 11:00 a.m., 10:15 a.m. and 10:50 a.m., respectively, and continued rising steadily due to tide coming up the estuary. These results indicated intrusions of saline water into the studied systems. In NW samples, the salinity in December 2020, April 2021, and August 2021

reached 6.25–14.70, 6.67–13.60, and 0.57–5.78, respectively. The degree of saltwater intrusion was more pronounced in the NW than in the EG samples ([Fig. 2A](#)), as salinity-related changes occurred more slowly in the microcosms due to the lag effect of a salinity equilibrium inside the dialysis bags. The average exchange efficiency of the dialysis bag was 0.16, 0.14 and 0.14 h^{-1} during three months, correspondingly ([Supplementary Table S5](#)).

Concentration of N species (NH_4^+ -N, NO_3^- -N, and NO_2^- -N) differed before vs. during saltwater intrusion as well as depending on the month. NH_4^+ concentrations in NW decreased in December ($P < 0.05$; 0.19–0.03 mg L^{-1}), but increased in August in all cases ($P < 0.05$, NW: 0.03–0.40 mg L^{-1} , EG: 0.13–0.32 mg L^{-1}), and in April there was no significant change ([Fig. 2A](#); [Supplementary Table S6](#)). NO_3^- patterns in NW and EG following saltwater intrusion were similar, as in all three experimental periods the NO_3^- concentration decreased ($P < 0.05$, [Fig. 2A](#)). NO_2^- concentrations in NW showed a slight but significant decreasing trend as the salinity increased in December ($P < 0.05$) whereas in the EG samples they sharply decreased after the saltwater intrusion in August ($P < 0.05$,

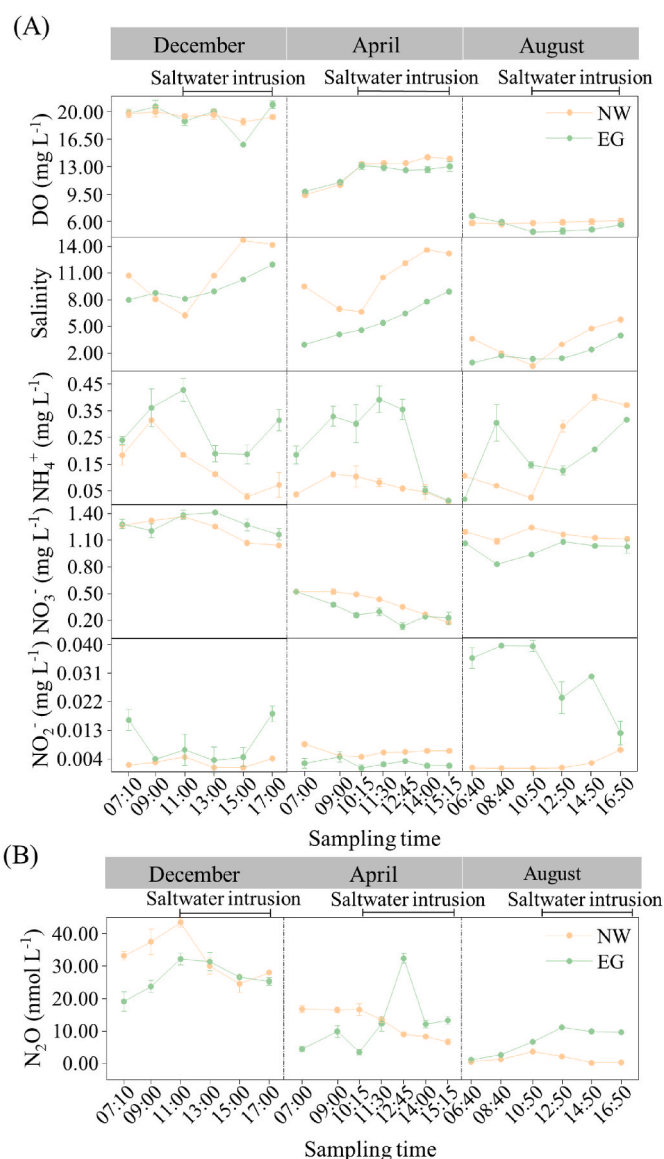


Fig. 2. Changes in DO, salinity and the concentrations of N components (A) and in the dynamics of dissolved N_2O (B) in NW (natural water surrounding the microcosms) and EG (experimental group: comprising microcosms set up in dialysis bags) at all sampling times in December, April, and August (A). Data represent the mean values of biological duplicates \pm standard deviation.

Fig. 2A; Supplementary Table S6).

3.2. Patterns of dissolved N_2O following saltwater intrusion and by month

Striking fluctuations in the dissolved N_2O concentration between the NW and EG samples were observed following the saltwater intrusions (Fig. 2B). In NW, the dissolved N_2O concentration decreased as the salinity increased in December and April and there was significant difference in the dissolved N_2O levels before and after saltwater intrusion ($P < 0.05$, Fig. 2B; Supplementary Table S6). During these two months, the dissolved N_2O levels at the beginning of the experiment were saturated (Supplementary Figs. S1A and B), and therefore the nitrogen conversion capacity was weak. Generally, marine water is much lower in N_2O than estuarine/river water. As such, after the saltwater intrusion, the mixing of marine water with the estuary have diluted the dissolved N_2O in the recipient environments, therefore leading to profound changes in N_2O level. In August, the dissolved N_2O was unsaturated, indicative of a stronger nitrogen conversion capacity, i.e., efficient consumption (Supplementary Fig. S1C). Nitrogen transformation is expected to be more intense in the unsaturated water. Hence, the dilution effect following saltwater intrusion and facilitated nitrogen transformation together did not result in a pronounced change in the dissolved N_2O . In the EG, the exchange with natural water outside of the dialysis bags was limited, and that might have weakened the dilution effect of low N_2O of the saltier water. The results showed a significant difference in dissolved N_2O before and after invasion for the EG group in April and August ($P < 0.05$, Fig. 2B; Supplementary Table S6). However, in December, due to limited nitrogen transformation capacity in saturated conditions (Fig. S1A), the differences in dissolved N_2O before and after saltwater intrusion were not evident.

Whether the dissolved N_2O concentration exhibited a seasonal pattern and the correlation of that pattern with the environmental parameters were also examined. Overall, the average concentration of dissolved N_2O over time was highest in December, followed by April and then August (Fig. 3 A). Dissolved N_2O concentrations were higher in NW (average $32.84 \text{ nmol L}^{-1}$) than in EG (average $26.43 \text{ nmol L}^{-1}$) in December ($P < 0.05$), but the opposite occurred in August ($P < 0.01$; NW: 1.34 nmol L^{-1} , EG: 6.84 nmol L^{-1}). N_2O concentration was negatively correlated to salinity in NW across all seasons ($P < 0.05$, Fig. 3B). Other physicochemical properties also affected NW during the three months. For example, pH correlated positively and negatively with dissolved N_2O in December and August, respectively. NH_4^+ correlated positively with dissolved N_2O in December and April ($P < 0.05$); NO_3^- correlated positively with dissolved N_2O in April and August ($P < 0.05$); and NO_2^- correlated negatively with dissolved N_2O in April ($P < 0.05$). In the EG samples, environmental factors played less of a role than in the NW samples, which contributed to the differences in the concentrations of dissolved N_2O during the three experimental periods. While salinity correlated negatively with the dissolved N_2O concentration in December ($P < 0.05$), temperature, NO_3^- , and NO_2^- correlated positively in different months and with varying degree of significance (Fig. 3B).

3.3. Salinity intrusion altered microbial community structure

Overall, based on OTU level, the bacterial communities in all samples were taxonomically distinct by month ($R < 0.59$ & $P < 0.01$, ANOSIM) and treatment ($R < 0.61$ & $P < 0.01$, ANOSIM; Supplementary Fig. S2A). Among the top 10 bacterial phyla in all samples, which together accounted for >92% of the microbial communities, *Proteobacteria* (36.24–85.08%), *Bacteroidota* (4.30–26.74%), *Actinobacteriota* (2.31–25.86%), and *Campilobacterota* (0.18–31.71%) were the dominant taxa (Supplementary Fig. S2B). Taxon representation at a finer scale was examined by screening the relative abundances of the 50 most numerous genera across samples. Regardless of the experimental month, 13 genera with higher relative abundances in EG than NW following saltwater intrusion (except in December) were shown to be involved in

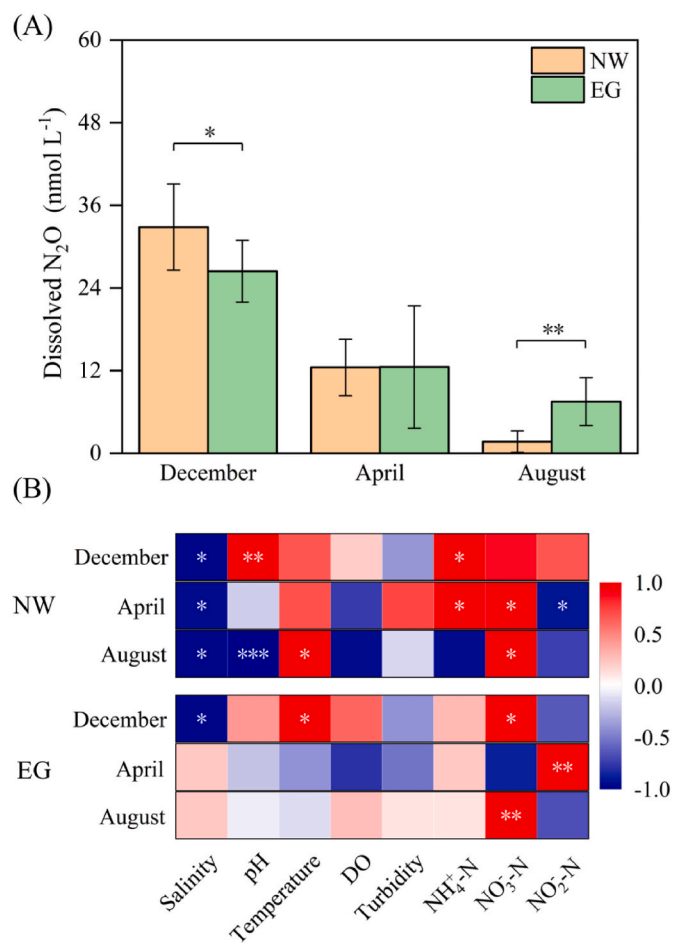


Fig. 3. Temporal variations in dissolved N_2O (A) and a Pearson correlation analysis of the relationship between dissolved N_2O concentration and environmental parameters (B). Color gradients in the heatmap represent the correlation, with warm colors (towards red) indicating a positive correlation and cold colors (towards blue) a negative correlation. Data represent the mean values \pm standard deviation. * $P < 0.05$; ** $P < 0.01$; *** $P < 0.001$. DO, dissolved oxygen.

denitrification (Xuan et al., 2022; Zhang et al., 2021) (Fig. 4, Supplementary Table S7). Denitrifying bacteria accounted for 0.33–75.00% of the bacterial communities in individual samples, among which *Vogesella* (0–20.05%) and *Flavobacterium* (0.12–21.86%) were most abundant (Supplementary Table S7). The *Flavobacterium* genome encodes all the enzymes needed to catalyze denitrification (Harter et al., 2016; Wang et al., 2016; Chen et al., 2021a). Among the top 50 genera, *Nitrospira* (0.01–2.77%) was the only nitrifier, and *Bacillus* (0–17.02%) is involved in DNRA (Fig. 4). In contrast to the denitrifiers, the relative abundances of those two genera were higher in NW than in EG following saltwater intrusion in April ($P < 0.05$) and in August ($P < 0.01$), respectively.

3.4. Changes of the functional gene abundance following salinity intrusion

Absolute abundances, expressed as gene copy numbers, were determined as a proxy for quantitative measurements of functional genes (Fig. 5 and in Supplementary Table S8, 'Absolute abundance'). In December, none of the N functional genes differed significantly in their absolute abundances between NW and EG (Fig. 5 and Supplementary Table S9). This result indicated that N transformation was limited because of the supersaturated state of N_2O in this month. In April, the absolute abundances of *nirK* (NW: 1.64×10^7 copies g^{-1} ; EG: 9.84×10^7 copies g^{-1}) and *nosZ* (NW: 2.79×10^6 copies g^{-1} ; EG: 1.81×10^8 copies g^{-1}), involved in denitrification, were significantly higher in EG than in

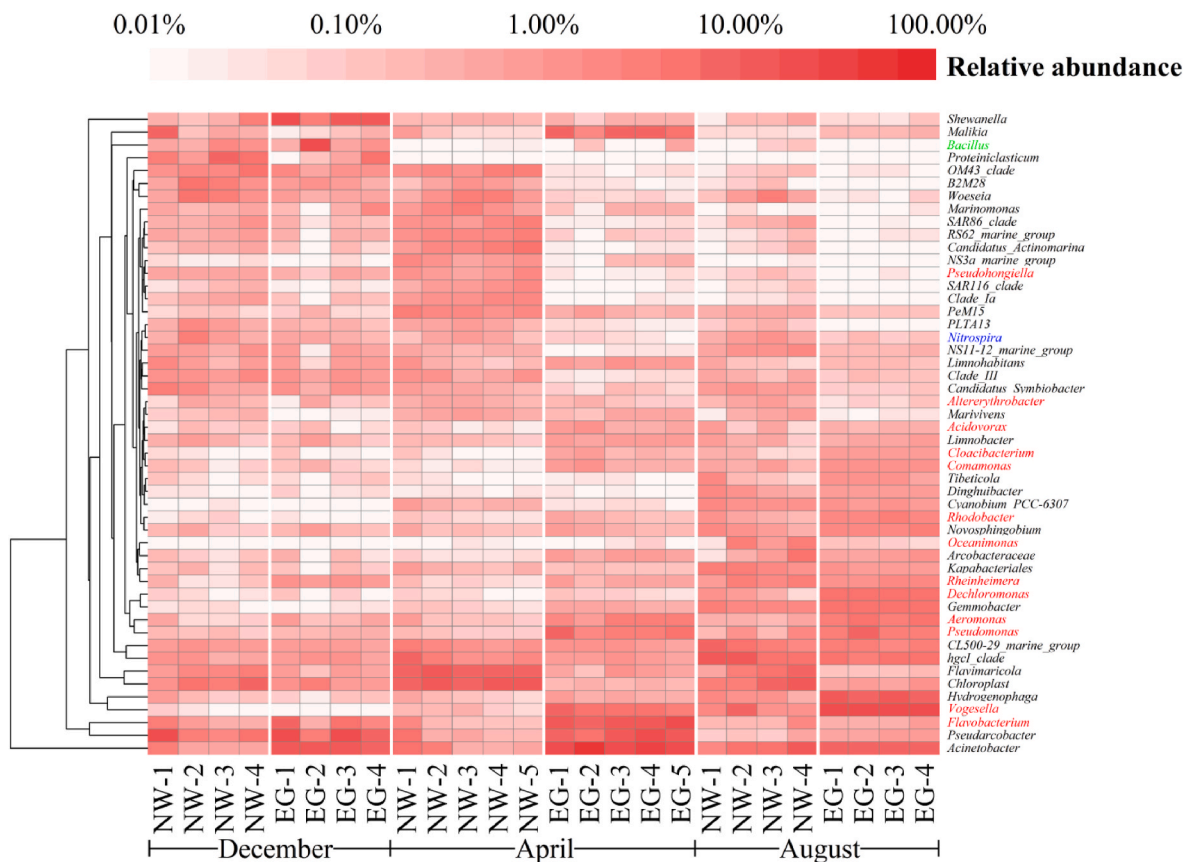


Fig. 4. Clustering of the 50 most abundant bacterial genera during a saltwater intrusion event across samples according to the abundance pattern. The heatmap shows the relative abundances of the genera by a color gradient. Bacterial genera are colored according to nitrogen conversion potential: nitrifiers in blue, denitrifiers in red, and dissimilatory nitrogen reducers in green. The data represent the average of biological duplicates.

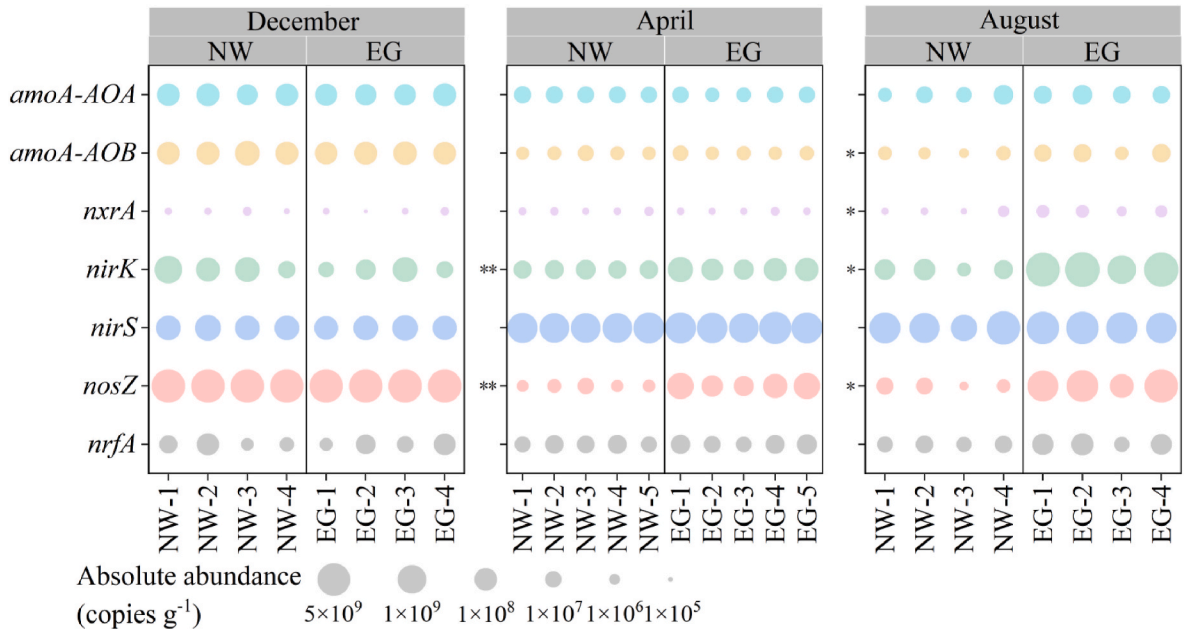


Fig. 5. Changes in the absolute abundances of functional genes involved in nitrification, denitrification, and DNRA following saltwater intrusion. Data are presented as the average of biological duplicates. Asterisks * indicate significant differences in gene quantification between the NW and EG (details on the statistical output are provided in [Supplementary Table S9](#)). * $P < 0.05$; ** $P < 0.01$.

NW ($P < 0.01$) (Fig. 5 and Supplementary Table S9). In August, the absolute abundances of *amoA-AOB*, *nirA*, *nirK*, and *nosZ* were higher in EG than in NW ($P < 0.05$, Fig. 5). A difference in 16S rRNA gene abundances between NW and EG was evident in April and August ($P < 0.05$), with higher abundances in EG than in NW (Supplementary Tables S8 and S9).

Linear regression analyses also showed differences in the correlations between dissolved N_2O concentrations and the absolute abundance of N-cycling genes (Fig. 6), reflecting differences in the relationship between the functional genes encoding nitrification, denitrification, or DNRA and the dissolved N_2O concentration. Thus, the abundances of *amoA-AOA*, *-AOB*, the main nitrification genes, correlated positively with dissolved N_2O in both NW and EG ($P < 0.01$), whereas *nirA* abundance correlated negatively with the dissolved N_2O concentration in EG ($P < 0.01$). Among the denitrification genes detected in NW, the abundances of both *nirK* and *nosZ* correlated significantly and positively with the dissolved N_2O concentration ($R^2 = 0.66$, $P < 0.01$ and $R^2 = 0.72$, $P < 0.01$, respectively); in EG, the opposite relationship was determined for *nirK* abundance ($R^2 = 0.58$, $P < 0.01$). A negative association was determined between *nirS* abundance and the dissolved N_2O concentration in both NW ($R^2 = 0.83$, $P < 0.001$) and EG ($R^2 = 0.87$, $P < 0.001$).

The relative abundance of each functional gene was estimated with respect to the absolute abundance of the 16S rRNA gene. Consistent with the absolute abundances of all functional genes, the relative abundances of *nirK*, *nirS*, and *nosZ*, were enriched in NW and EG compared to other genes during the three months (Supplementary Fig. S3). In most cases, these denitrification genes were more abundant than *nirA* ($P < 0.05$ or $P < 0.01$; Supplementary Table S10). For nitrification genes, the relative

abundances of *amoA-AOB* and *amoA-AOA* were significantly lower than that of the denitrification genes in the EG, such as *nirK* and *nirS*, while such difference was not observed in NW ($P < 0.05$, Supplementary Fig. S3 and Table S10).

4. Discussion

4.1. Impact of physicochemical properties on N_2O dynamics during salinity intrusion in different months

Dissolved N_2O in estuaries can act as both source and sink for atmospheric N_2O (Li et al., 2022). In this study, the dissolved N_2O concentration ranged from 0.16 to 43.50 nmol L^{-1} , with significant tidal and seasonal variations. That salinity is a primary environmental stressor influencing microbial diversity, functional diversity, and biogeochemical cycles is well-established (Shen et al., 2018a; Herbert et al., 2015; Herbert et al. 2015, 2015). Our study showed a strong negative correlation between the dissolved N_2O concentration and salinity in December. While in April and August, both the dissolved N_2O concentration and N_2O saturation increased following saltwater intrusion. This result corroborates our previous finding that a salt pulse increases the solubility of accumulated N_2O in water (Xie et al., 2020). However, when dissolved N_2O reached stable supersaturation, the increase in the solubility triggered by salt pulse is limited.

The differences in the dissolved N_2O concentrations between the NW and EG samples can be explained by several processes. First, the impact of the abiotic conditions such as salinity and nitrogen concentrations inside the dialysis bags might have been delayed whereas in NW the changes accompanying the saltwater inflow had direct effects. Second,

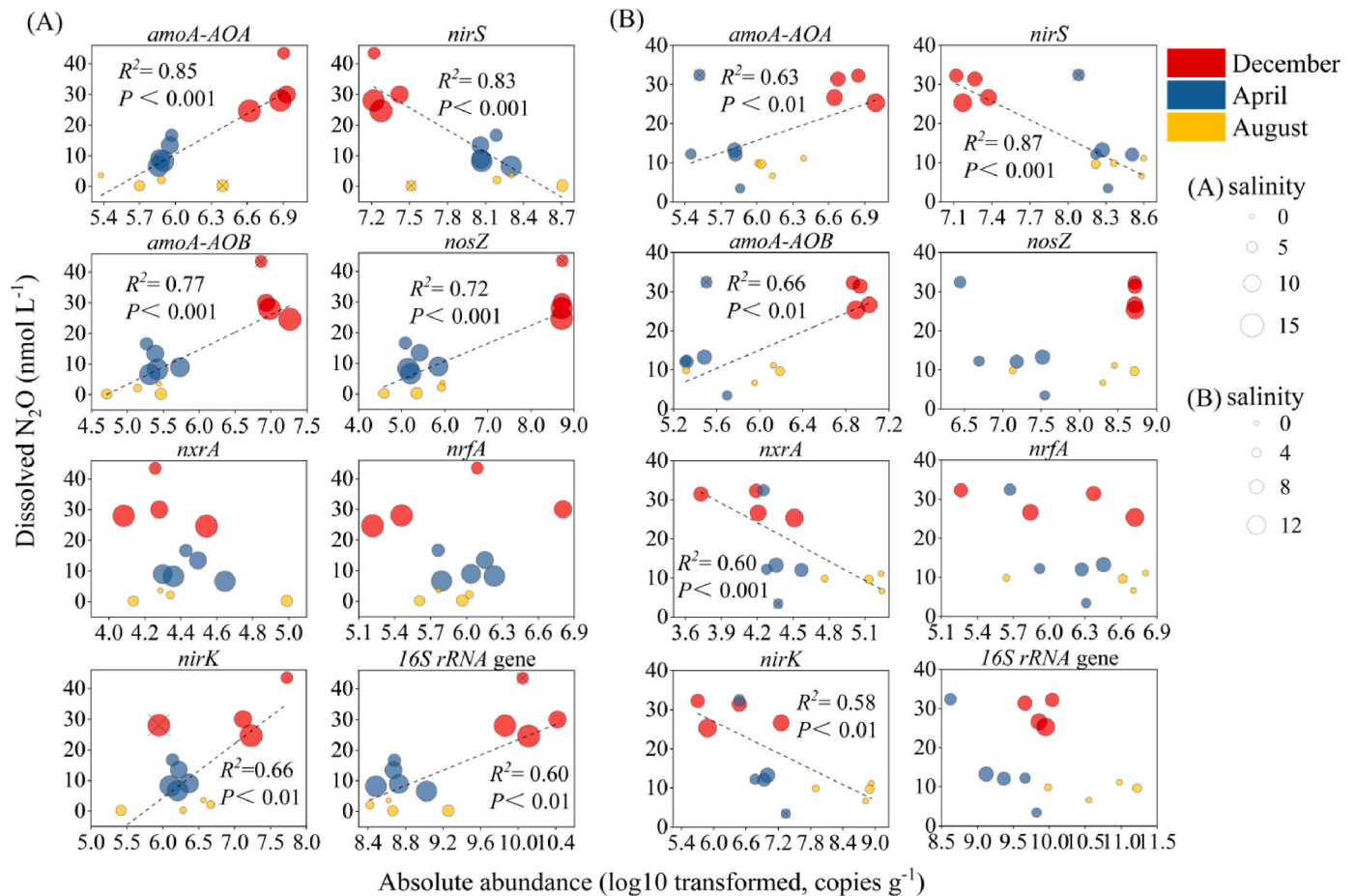


Fig. 6. Linear regression analyses illustrating the relationship between functional gene abundances and the dissolved N_2O concentration in NW (A) and EG (B). Dashed lines represent the best fit of the regression; dots with \times were excluded from the correlation analysis.

although the microbial communities in both NW and EG were exposed to a change in the environmental conditions, the perception of those changes by the communities differed, as the ecosystems in NW and the microcosms differed in their size, and the environmental fluctuations in each ecosystem are size-dependent (Bier et al., 2022). In addition, the confounding effects, such as the speed of water flow, interplay of the physiochemical parameters surveyed, and the active state of microbial individuals accompanied of saltwater intrusion, have different impacts on the N transformation and the microbial activity involved depending on ecosystem size. Third, NW additionally received an input of microbes via the saltwater intrusion. The exchange of entire communities that accompanies a change in environmental matrixes is referred to as coalescence (Rillig et al., 2015; Izabel-Shen, 2021). Last, NW could be in contact with sediment, but microcosms were not. Presumably, the input of microbes and nutrients from the saltwater intrusion and/or sediment had functional consequences for the recipient community (competition or facilitation) in NW, resulting in a trajectory of the N_2O dynamics that differed from that in the microcosms.

In the field, many factors besides salinity interact in complex ways that affect the temporal changes in dissolved N_2O (Grossel et al., 2021). Temperature had a strong positive effect on the dissolved N_2O in December but relatively weak and potentially negative effects in April and August (Fig. 3B), indicative of a dual effect of temperature on the dissolved N_2O level. Thus, while high temperatures can reduce the solubility of N_2O (Zhang et al., 2008), they can also facilitate nitrification and denitrification and thereby stimulate the production of dissolved N_2O (Weiss and Price, 1980; Walter et al., 2006). Noteworthy, both the dissolved N_2O concentration and N_2O saturation in December appeared to be higher than that in April and August, showing temperature-dependence. In most natural systems, saltwater intrusion carries salt- and oxygen-rich waters (Feistel et al., 2016). However, there was no correlation between the DO and dissolved N_2O concentrations in either NW or EG and the degree of saltwater intrusion did not significantly change the diurnal DO level (Supplementary Table S3). The significant positive correlation between the NO_3^- and N_2O concentrations in both NW and EG suggested that denitrification is a significant process that drives N_2O production and consumption (Beaulieu et al., 2011; Zhou et al., 2022). The significant positive correlation between NH_4^+ and the dissolved N_2O concentration only in NW not in EG suggested that N_2O dynamics in natural estuarine environments reflect the combined effects of nitrification, denitrification (and DNRA).

The source-sink dynamics of N_2O can be estimated from the saturation rate. In our study, the release and accumulation of dissolved N_2O in the estuary were seasonality dependent. N_2O saturation ranged from 145.27% to 377.13% in December, from 18.87% to 349.45% in April, and from 2.27% to 167.38% in August. Interestingly, the patterns of N_2O saturation in NW contrasted with those in the microcosms following saltwater intrusion (Supplementary Fig. S1). For instance, N_2O was undersaturated (i.e.; saturation <100%) in the microcosms before the saltwater intrusions but oversaturated thereafter, indicative of a sink-to-source transition of N_2O dynamics. By contrast, NW went from being a source to a potential sink of N_2O , given the low level of N_2O saturation following the intrusion. These results suggest a significant contribution of saltwater intrusions to the release and accumulation of dissolved N_2O in the estuary. They further suggest that, in contrast to open water, semi-closed environments with a relatively low water velocity, as mimicked by the field microcosms, could act as a source of N_2O . Indeed, coastal wetlands or lagoons are a natural source of N_2O , as they respond to tidal influences on the movement and distribution of water and salinity, as noted elsewhere (Moseman-Valtierra et al., 2011; Rosentreter et al., 2021).

We found seasonality of the dissolved N_2O , with highest in December, followed by April and August both in NW and EG samples. The results suggested that the high temperature reduces the solubility of N_2O . In warm seasons like August in our study, the N_2O emissions are generally higher (Wang et al., 2007; Allen et al., 2011; Lin et al., 2016).

However, direct solubility effect was limited as lower fluxes were also exhibited in summer and autumn compared to that in spring and winter. Furthermore, the excess nitrogen from fertilizer application, pollution discharge, and water regulations outflow discharges from rivers to coastal waters has significantly increased in past decades, which altogether mediate N speciation and N transformation. As such, the season changes in NH_4^+ and NH_3 can play important roles in the N_2O variations (Bouwman et al., 2005; Liu et al., 2019). We found positive correlations between NH_4^+ , NH_3 , and the dissolved N_2O concentrations in all three months. Specifically, the increase in the dissolved N_2O concentrations related to high concentrations of NH_4^+ and NH_3 ; the processes involved with the latter two were attributed to the N_2O production in the water.

4.2. Impact of biological changes on dissolved N_2O

Nitrification and denitrification are regulated by microbial respiration and microbially mediated enzyme activity, both of which are sensitive to changes in salinity (Weston et al., 2011; Morrissey et al., 2014; Li et al., 2019). In this study, the increases in *nir* gene abundances were much larger than the increases in genes involved in nitrification and DNRA following saltwater intrusion. The enrichment of *nosZ* in both NW and EG during the intrusion event suggested that the activity of this gene is enhanced by a high salinity (Wang et al., 2018; Li et al., 2019). The abundances of these denitrification genes were also higher in the microcosms than in NW (Fig. 5), and similar patterns were observed for the dissolved N_2O concentration. *nirK* and *nirS* encode two different nitrite reductases (Zhao et al., 2018a). The higher oxygen tolerance of *nirK* denitrifiers than *nirS* denitrifiers ensures the activity of the former even in high DO environments (Knapp et al., 2009; Song et al., 2022), as observed in this study. Our previous work also demonstrated an increase in *nirK* abundance with rising salinity that drove N_2O production (Xie et al., 2020). In addition to denitrification as a significant driver of the production and consumption of dissolved N_2O in our study, there may well be other sources of N_2O whose contributions to the observed differences in the dissolved N_2O in the NW and EG samples in this study remain to be determined.

These other sources of N_2O may represent nitrifier-dominated denitrification, as nitrifiers can produce N_2O via unique enzyme activities. Both AOA and AOB produce N_2O from NO_2^- (Stieglmeier et al., 2014; Jung et al., 2014). Given their high affinity for NH_4^+-N , AOA outcompete AOB when the ambient NH_4^+ is low (Hink et al., 2017; Wrage-Mönnig et al., 2018). Like AOA, comammox *Nitrospira*, which are complete nitrifying bacteria, are favored under low NH_4^+ . In this study, the NH_4^+ concentration was <0.5 mg/L across samples and *Nitrospira* were more abundant in NW than in the microcosms, where the NH_4^+ concentration was 2-fold higher (Figs. 2 and 4). In addition, the abundances of *amoA* genes from AOA and AOB correlated significantly with the dissolved N_2O concentration (Fig. 6). Overall, these results suggest that nitrifiers, comprising AOA, comammox *Nitrospira*, and AOB, are additional sources of N_2O production in NW. As there was no significant association between *nrfA* gene abundance and the dissolved N_2O concentration, N_2O produced as a by-product of DNRA was presumably negligible.

Along with production, the net dissolved N_2O concentration is the result of N_2O consumption, with *nosZ* as the key gene mitigating N_2O emissions. *nosZ* encodes a nitrous oxide reductase that participates in biological denitrification, thus reducing the powerful greenhouse gas N_2O to harmless N_2 (Kuypers et al., 2018). Interestingly, *nosZ* gene abundance correlated significantly with the dissolved N_2O concentration in NW but not in EG. Although *nosZ* gene abundance was greater in the latter (Fig. 5), *nosZ* activity in the EG may have been limited by the delayed effect of the dialysis bag, i.e., the delaying impact of the abiotic conditions on the water inside compared to outside the bag or by abiotic or biotic conditions not measured in this study. In NW, the saltwater intrusion may have caused the majority of the produced N_2O to be efficiently converted into gaseous N_2 , which was further supported by

the rates of N₂O saturation. However, the temporal patterns of the dissolved N₂O in the three months indicated that the Minjiang estuary acts as both source and sink of N₂O due to the balance between the microbial mediation and physical exchange caused by the salinity intrusion.

5. Conclusions

This study investigated the temporal patterns of dissolved N₂O dynamics in Minjiang estuary, which undergoes regular saltwater intrusions. We found that the changes in the environment induced by saltwater intrusion and month affected the dissolved N₂O concentration. The higher N₂O concentrations in field microcosms than in NW may have been the result of the limited N₂O consumption in the former, as indicated by the absence of an association with *nosZ* gene abundance. Although classic denitrification was a significant driver of N₂O production and consumption in our study, nitrifier-driven denitrification process may provide an additional source of N₂O, given the strong association between *amoA* genes and the abundance of *Nitrospira*. Further studies should be directed at determining the rates of microbial N₂O production and consumption, such as by isotopic tracing, and at the identification of metabolic pathways by meta-transcriptome analysis. The results will yield insights into the interactions of N cyclers and thus the regulation of N₂O production and emission in estuarine environments.

CRedit authorship contribution statement

Rongrong Xie: Conceptualization, Funding acquisition, Methodology, Supervision, Writing - review & editing. **Laichang Lin:** Data curation, Investigation, Writing - original draft. **Chengchun Shi:** Resources, Supervision. **Peng Zhang:** Methodology. **Peiyuan Rao:** Data curation, Formal analysis, Investigation. **Jiabing Li:** Supervision, Validation. **Dandan Izabel-Shen:** Data curation, Methodology, Writing - original draft, Writing - review & editing.

Declaration of competing interest

The authors declare that they have no known competing financial interests or personal relationships that could have appeared to influence the work reported in this paper.

Data availability

The sequencing data were deposited in the NCBI database with Bioproject number PRJNA967111. Other data will be made available on request.

Acknowledgments

This work was partially supported by the National Natural Science Foundation of China (42007343) and the Fujian Provincial Natural Science Foundation (2021J01195). We express our especial thanks to Prof. Zuliang Chen for providing supports on field sampling and comments on early manuscript drafts.

Appendix A. Supplementary data

Supplementary data to this article can be found online at <https://doi.org/10.1016/j.envres.2023.118021>.

References

Allen, D., Dalal, R.C., Rennenberg, H., Schmidt, S., 2011. Seasonal variation in nitrous oxide and methane emissions from subtropical estuary and coastal mangrove sediments, Australia. *Plant Biol.* 13, 126–133.
Bange, H.W., 2006. Nitrous oxide and methane in European coastal waters. *Estuar. Coast Shelf Sci.* 70, 361–374.

Bange, H.W., 2008. Gaseous Nitrogen Compounds (NO, N₂O, N₂, NH₃) in the Ocean. Elsevier Inc., p. 51–94.
Bange, H.W., Sim, C.H., Bastian, D., Kallert, J., Kock, A., Mujahid, A., Mueller, M., 2019. Nitrous oxide (N₂O) and methane (CH₄) in rivers and estuaries of northwestern Borneo. *Biogeosciences* 16, 4321–4335.
Barlow, P.M., Reichard, E.G., 2010. Saltwater intrusion in coastal regions of North America. *Hydrogeol. J.* 18, 247–260.
Beaulieu, J.J., Tank, J.L., Hamilton, S.K., Wollheim, W.M., Hall, R.O., Mulholland, P.J., Peterson, B.J., Ashkenas, L.R., Cooper, L.W., Dahm, C.N., Dodds, W.K., Grimm, N.B., Johnson, S.L., McDowell, W.H., Poole, G.C., Valett, H.M., Arango, C.P., Bernot, M.J., Burgin, A.J., Crenshaw, C.L., Helton, A.M., Johnson, L.T., O'Brien, J.M., Potter, J.D., Sheibley, R.W., Sobota, D.J., Thomas, S.M., 2011. Nitrous oxide emission from denitrification in stream and river networks. *Proc. Natl. Acad. Sci. U.S.A.* 108, 214–219.
Bier, R.L., Vass, M., Székely, A.J., et al., 2022. Ecosystem size-induced environmental fluctuations affect the temporal dynamics of community assembly mechanisms. *ISME J.* 16 (12), 2635–2643.
Bolger, A.M., Lohse, M., Usadel, B., 2014. Trimmomatic: a flexible trimmer for Illumina sequence data. *Bioinformatics* 30, 2114–2120.
Bouwman, A.F., Van Drecht, G., Knoop, J.M., Beusen, A.H.W., Meinardi, C.R., 2005. Exploring changes in river nitrogen export to the world's oceans. *Global Biogeochem* 19, GB1002.
Chen, F.M., Li, G.W., Li, X.G., 2021a. The cotreatment of old landfill leachate and domestic sewage in rural areas by deep subsurface wastewater infiltration system (SWIS): performance and bacterial community. *Environ. Pollut.* 274, 1–10.
Chen, M., Pan, H., Sun, M., He, W., Wei, M., Lou, Y., et al., 2021b. Nitrospira cluster 3 lineage of AOB and nirK of rhizobiales respectively dominated N₂O emissions from nitrification and denitrification in organic and chemical N fertilizer treated soils. *Ecol. Indic.* 127, 107722.
Church, J.A., Clark, P.U., Cazenave, A., Gregory, J.M., Jevrejeva, S., Levermann, A., Merrifield, M.A., Milne, G.A., Nerem, R.S., Nunn, P.D., Payne, A.J., Pfeffer, W.T., Stammer, D., Unnikrishnan, A.S., 2013. Sea-level rise by 2100. *Science* 342, 1445–1445.
Comer-Warner, S.A., Ullah, S., Dey, A., Stagg, C.L., Elsey-Quirk, T., Swarzenski, C.M., Sgouridis, F., Krause, S., Chmura, G.L., 2023. Elevated temperature and nutrients lead to increased N₂O emissions from salt marsh soils from cold and warm climates. *Biogeochemistry*.
Cooper, R.J., Wexler, S.K., Adams, C.A., Hiscock, K.M., 2017. Hydrogeological controls on regional-scale indirect nitrous oxide emission factors for rivers. *Environ. Sci. Technol.* 51, 10440–10448.
Feistel, S., Feistel, R., Nehring, D., Matthäus, W., Nausch, G., Naumann, M., 2016. Hypoxic and Anoxic Regions in the Baltic Sea, 1969–2015. *Meereswiss. Ber., Warnemünde*, p. 100.
Franklin, R.B., Morrissey, E.M., Morina, J.C., 2017. Changes in abundance and community structure of nitrate-reducing bacteria along a salinity gradient in tidal wetlands. *Pedobiologia* 60, 21–26.
Grossel, A., Bourennane, H., Ayzac, A., Pasquier, C., Hénault, C., 2021. Indirect emissions of nitrous oxide in a cropland watershed with contrasting hydrology in central France. *Sci. Total Environ.* 766, 142664.
Han, P., Wu, D., Sun, D., Zhao, M., Wang, M., Wen, T., Zhang, J., Hou, L., Liu, M., Klumper, U., Zheng, Y., Dong, H.P., Liang, X., Yin, G., 2021. N₂O and NO_y production by the comammox bacterium Nitrospira inopinata in comparison with canonical ammonia oxidizers. *Water Res.* 190, 116728.
Harley, J.F., Carvalho, L., Dudley, B., Heal, K.V., Rees, R.M., Skiba, U., 2015. Spatial and sea-seasonal fluxes of the greenhouse gases N₂O, CO₂ and CH₄ in a UK macrotidal estuary. *Estuar. Coast Shelf Sci.* 153, 62–73.
Harter, J., Weigold, P., El-Hadidi, M., Huson, D.H., Kappler, A., Behrens, S., 2016. Soil biochar amendment shapes the composition of N₂O-reducing microbial communities. *Sci. Total Environ.* 562, 379–390.
Henry, S., Bru, D., Stres, B., Hallet, S., Philippot, L., 2006. Quantitative detection of the *nosZ* gene, encoding nitrous oxide reductase, and comparison of the abundances of 16S rRNA, *narG*, *nirK*, and *nosZ* genes in soils. *Appl. Environ. Microbiol.* 72, 5181–5189.
Herbert, E.R., Boon, P., Burgin, A.J., Neubauer, S.C., Franklin, R.B., Ardón, M., Hopfensperger, K.N., Lamers, L.P.M., Gell, P., 2015. A global perspective on wetland salinization: ecological consequences of a growing threat to freshwater wetlands. *Ecosphere* 6, art206.
Hink, L., Lycus, P., Gubry-Rangin, C., Frostegård, Å., Nicol, G.W., Prosser, J.I., Bakken, L.R., 2017. Kinetics of NH₃-oxidation, NO₃-turnover, N₂O-production and electron flow during oxygen depletion in model bacterial and archaeal ammonia oxidisers. *Environ. Microbiol.* 19, 4882–4896.
Hu, H.-W., Chen, D., He, J.-Z., 2015. Microbial regulation of terrestrial nitrous oxide formation: understanding the biological pathways for prediction of emission rates. *FEMS Microbiol. Rev.* 39 (5), 729–749.
Huertas, L.E., Flecha, S., Navarro, G., Perez, F.F., de la Paz, M., 2018. Spatio-temporal variability and controls on methane and nitrous oxide in the Guadalquivir Estuary, Southwestern Europe. *Aquat. Sci.* 80, 29.
Izabel-Shen, D., 2021. Understanding response of microbial communities to saltwater intrusion through microcosms. *Comput. Struct. Biotechnol. J.* 19, 929–933.
Jung, M.Y., Well, R., Min, D., Giesemann, A., Park, S.J., Kim, J.G., Kim, S.J., Rhee, S.K., 2014. Isotopic signatures of N₂O produced by ammonia-oxidizing archaea from soils. *ISME J.* 8, 1115–1125.
Kits, K.D., Jung, M.-Y., Vierheilig, J., Pjevac, P., Sedlacek, C.J., Liu, S., Herbold, C., Stein, L.Y., Richter, A., Wissel, H., Brüggemann, N., Wagner, M., Daims, H., 2019. Low yield and abiotic origin of N₂O formed by the complete nitrifier Nitrospira inopinata. *Nat. Commun.* 10 (1), 1836.

- Knapp, C.W., Dodds, W.K., Wilson, K.C., O'Brien, J.M., Graham, D.W., 2009. Spatial heterogeneity of denitrification genes in a highly homogenous urban stream. *Environ. Sci. Technol.* 43, 4273–4279.
- Kozlowski, J.A., Price, J., Stein, L.Y., 2014. Revision of N_2O -producing pathways in the ammonia-oxidizing bacterium *Nitrosomonas europaea* ATCC 19718. *Appl. Environ. Microbiol.* 80, 4930–4935.
- Kuypers, M.M.M., Marchant, H.K., Kartal, B., 2018. The microbial nitrogen-cycling network. *Nat. Rev. Microbiol.* 16, 263.
- Levy-Booth, D.J., Prescott, C.E., Grayston, S.J., 2014. Microbial functional genes involved in nitrogen fixation, nitrification and denitrification in forest ecosystems. *Soil Biol. Biochem.* 75, 11–25.
- Li, X., Gao, D., Hou, L., Liu, M., 2019. Salinity stress changed the biogeochemical controls on CH_4 and N_2O emissions of estuarine and intertidal sediments. *Sci. Total Environ.* 652, 593–601.
- Li, X., Qi, M., Gao, D., Liu, M., Sardans, J., Peñuelas, J., Hou, L., 2022. Nitrous oxide emissions from subtropical estuaries: insights for environmental controls and implications. *Water Res.* 212, 118110.
- Lin, H., Dai, M., Kao, S.J., Wang, L., Roberts, E., Yang, J.Y.T., Huang, T., He, B., 2016. Spatiotemporal variability of nitrous oxide in a large eutrophic estuarine system: the Pearl River Estuary, China. *Mar. Chem.* 182, 14–24.
- Liu, S., Xie, Z.H., Zeng, Y.J., Liu, B., Li, R.C., Wang, Y., Wang, L.H., Qin, P.H., Jia, B.H., Xie, J.B., 2019. Effects of anthropogenic nitrogen discharge on dissolved inorganic nitrogen transport in global rivers. *Global Change Biol.* 25, 1493–1513.
- Ma, L., Lin, H., Xie, X., Dai, M., Zhang, Y., 2019. Major role of ammonia-oxidizing bacteria in N_2O production in the Pearl River estuary. *Biogeochemistry* 16, 4765–4781.
- Morrissey, E.M., Gillespie, J.L., Morina, J.C., Franklin, R.B., 2014. Salinity affects microbial activity and soil organic matter content in tidal wetlands. *Global Change Biol.* 20, 1351–1362.
- Moseman-Valtierra, S., Gonzalez, R., Kroeger, K.D., Tang, J., Chao, W.C., Crusius, J., Bratton, J., Green, A., Shelton, J., 2011. Short-term nitrogen additions can shift a coastal wetland from a sink to a source of N_2O . *Atmos. Environ.* 45, 4390–4397.
- Murray, R.H., Erler, D.V., Eyre, B.D., 2015. Nitrous oxide fluxes in estuarine environments: response to global change. *Global Change Biol.* 21, 3219–3245.
- Murray, R.H., Erler, D.V., Rosentreter, J., Wells, N.S., Eyre, B.D., 2020. Seasonal and spatial controls on N_2O concentrations and emissions in low-nitrogen estuaries: evidence from three tropical systems. *Mar. Chem.* 221, 103779.
- Nebbioso, A., Piccolo, A., 2013. Molecular characterization of dissolved organic matter (DOM): a critical review. *Anal. Bioanal. Chem.* 405, 109–124.
- Rillig, M.C., Antonovics, J., Caruso, T., Lehmann, A., Powell, J.R., Veresoglou, S.D., Verbruggen, E., 2015. Interchange of entire communities: microbial community coalescence. *Trends Ecol. Evol.* 30, 470–476.
- Rosamond, M.S., Thuss, S.J., Schiff, S.L., 2012. Dependence of riverine nitrous oxide emissions on dissolved oxygen levels. *Nat. Geosci.* 5, 715–718.
- Rosentreter, J.A., Al-Haj, A.N., Fulweiler, R.W., Williamson, P., 2021. Methane and nitrous oxide emissions complicate coastal blue carbon assessments. *Global Biogeochem. Cycles* 35, e2020GB006858.
- Santoro, A.E., 2010. Microbial nitrogen cycling at the saltwater–freshwater interface. *Hydrogeol. J.* 18, 187–202.
- Santoro, A.E., Buchwald, C., McIlvin, M.R., Casciotti, K.L., 2011. Isotopic signature of N_2O produced by marine ammonia-oxidizing archaea. *Science* 333 (6047), 1282–1285.
- Shen, D., Langenheder, S., Jürgens, K., 2018a. Dispersal modifies the diversity and composition of active bacterial communities in response to a salinity disturbance. *Front. Microbiol.* 9, 2188.
- Shen, D., Jürgens, K., Beier, S., 2018b. Experimental insights into the importance of ecologically dissimilar bacteria to community assembly along a salinity gradient. *Environ. Microbiol.* 20, 1170–1184.
- Sierra, A., Jimenez-Lopez, D., Ortega, T., Ponce, R., Bellanco, M.J., Sanchez-Leal, R., Gomez-Parra, A., Forja, J., 2017. Distribution of N_2O in the eastern shelf of the gulf of Cadiz (SW Iberian Peninsula). *Sci. Total Environ.* 593, 796–808.
- Song, K., Senbati, Y., Li, L., Zhao, X., Xue, Y., Deng, M., 2022. Distinctive microbial processes and controlling factors related to indirect N_2O emission from agricultural and urban rivers in taihu watershed. *Environ. Sci. Technol.* 56, 4642–4654.
- Stieglmeier, M., Mooshammer, M., Kitzler, B., Wanek, W., Zechmeister-Boltenstern, S., Richter, A., Schleper, C., 2014. Aerobic nitrous oxide production through N-nitrosating hybrid formation in ammonia-oxidizing archaea. *ISME J.* 8, 1135–1146.
- Su, X., Yang, L., Yang, K., Tang, Y., Wen, T., Wang, Y., Rillig, M.C., Rohe, L., Pan, J., Li, H., Zhu, Y., 2022. Estuarine plastisphere as an overlooked source of N_2O production. *Nat. Commun.* 13, 3884.
- Theodorakopoulos, N., Lognoul, M., Degruene, F., Broux, F., Regaert, D., Muys, C., Heinesch, B., Bodson, B., Aubinet, M., Vandenbol, M., 2017. Increased expression of bacterial amoA during an N_2O emission peak in an agricultural field. *Agric. Ecosyst. Environ.* 236, 212–220.
- UNESCO, 1985. The international system of units (SI) in oceanography. *Unesco Tech. Pap. Arine Sci.* 45, 43.
- Walter, S., Breitenbach, U., Bange, H.W., Nausch, G., Wallace, D.W.R., 2006. Distribution of N_2O in the Baltic Sea during transition from anoxic to oxic conditions. *Biogeochemistry* 3, 557–570.
- Wan, X.S., Hou, L., Kao, S.-J., Zhang, Y., Sheng, H.-X., Shen, H., Tong, S., Qin, W., Ward, B.B., 2023. Pathways of N_2O production by marine ammonia-oxidizing archaea determined from dual-isotope labeling. *Proc. Natl. Acad. Sci. USA* 120, e2220697120.
- Wang, D., Chen, Z., Wang, J., Xu, S., Yang, H., Chen, H., Yang, L., Hu, L., 2007. Summer-time denitrification and nitrous oxide exchange in the intertidal zone of the Yangtze Estuary. *Estuar. Coast Shelf Sci.* 73 (1–2), 43–53.
- Wang, H., Gilbert, J.A., Zhu, Y., Yang, X., 2018. Salinity is a key factor driving the nitrogen cycling in the mangrove sediment. *Sci. Total Environ.* 631–632, 1342–1349.
- Wang, J., Song, X., Wang, Y., Abayneh, B., Li, Y., Yan, D., Bai, J., 2016. Nitrate removal and bioenergy production in constructed wetland coupled with microbial fuel cell: establishment of electrochemically active bacteria community on anode. *Bioresour. Technol.* 221, 358–365.
- Wanninkhof, R., 1992. Relationship between wind speed and gas exchange over the ocean. *J. Geophys. Res.* 97, 7373.
- Weiss, R.F., Price, B.A., 1980. Nitrous oxide solubility in water and seawater. *Mar. Chem.* 347–359.
- Wells, N.S., Maher, D.T., Erler, D.V., Hipsey, M., Rosentreter, J.A., Eyre, B.D., 2018. Estuaries as sources and sinks of N_2O across a land use gradient in subtropical Australia. *Global Biogeochem. Cycles* 32 (5), 877–894.
- Weston, N.B., Vile, M.A., Neubauer, S.C., Velinsky, D.J., 2011. Accelerated microbial organic matter mineralization following salt-water intrusion into tidal freshwater marsh soils. *Biogeochemistry* 102, 135–151.
- Wolanski, E., Elliott, M., 2015. *Estuarine Ecohydrology: an Introduction*, second ed. Elsevier Science, Amsterdam, Oxford.
- Woodward, W., Appell, G., 1986. Current velocity measurements using acoustic Doppler backscatter: a review. *IEEE J. Ocean. Eng.* 11, 3–6.
- Wrage, N., Velthof, G.L., van Beusichem, M.L., et al., 2001. Role of nitrifier denitrification in the production of nitrous oxide. *Soil Biol. Biochem.* 33, 1723–1732.
- Wrage-Mönning, N., Horn, M.A., Well, R., Muller, C., Velthof, G., Oenema, O., 2018. The role of nitrifier denitrification in the production of nitrous oxide revisited. *Soil Biol. Biochem.* 123, A3–A16.
- Xia, X.H., Jia, Z.M., Liu, T., Zhang, S.B., Zhang, L.W., 2017. Coupled nitrification-denitrification caused by suspended sediment (SPS) in rivers: importance of SPS size and composition. *Environ. Sci. Technol.* 51, 212–221.
- Xie, R., Qi, J., Shi, C., Zhang, P., Wu, R., Li, J., Wanick, J.J., 2023. Salt intrusion alters nitrogen cycling in tidal reaches as determined in field and laboratory investigations. *Sci. Total Environ.* 800, 163251.
- Xie, R., Rao, P., Pang, Y., Shi, C., Li, J., Shen, D., 2020. Salt intrusion alters nitrogen cycling in tidal reaches as determined in field and laboratory investigations. *Sci. Total Environ.* 729, 138803.
- Xie, R., Pang, Y., Luo, B., Li, J., Wu, C., Zheng, Y., Sun, Q., Zhang, P., Wang, F., 2017. Spatiotemporal variability in salinity and hydraulic relationship with salt intrusion in the tidal reaches of the Minjiang River, Fujian Province, China. *Environ. Sci. Pollut. Res.* 24, 11847–11855.
- Xuan, Y., Mai, Y., Xu, Y., Zheng, J., He, Z., Shu, L., Cao, Y., 2022. Enhanced microbial nitrification-denitrification processes in a subtropical metropolitan river network. *Water Res.* 222, 118857.
- Zhang, G., Zhang, J., Ren, J., Li, J., Liu, S., 2008. Distributions and sea-to-air fluxes of methane and nitrous oxide in the North East China Sea in summer. *Mar. Chem.* 110, 42–55.
- Zhang, L., Wang, L., Yin, K.D., Lü, Y., Zhang, D.R., Yang, Y.Q., Huang, X.P., 2013. Pore water nutrient characteristics and the fluxes across the sediment in the Pearl River estuary and adjacent waters. *China. Estuar. Coastal Shelf S.* 133, 182–192.
- Zhang, M., Wang, Z.-J., Huang, J.-C., Sun, S., Cui, X., Zhou, W., He, S., 2021. Salinity-driven nitrogen removal and its quantitative molecular mechanisms in artificial tidal wetlands. *Water Res.* 202, 117446.
- Zhang, J., Kobert, K., Flouri, T., Stamatakis, A., 2014. PEAR: a fast and accurate Illumina Paired-End reAd mergeR. *Bioinformatics* 30, 614–620.
- Zhao, B., Cheng, D.Y., Tan, P., An, Q., Guo, J.S., 2018a. Characterization of an aerobic denitrifier *Pseudomonas stutzeri* strain XL-2 to achieve efficient nitrate removal. *Bioresour. Technol.* 250, 564–573.
- Zhao, S., Wang, Q., Zhou, J., Yuan, D., Zhu, G., 2018b. Linking abundance and community of microbial N_2O -producers and N_2O -reducers with enzymatic N_2O production potential in a riparian zone. *Sci. Total Environ.* 642, 1090–1099.
- Zhen, L., Wu, X., Li, J., Xie, R., 2022. Component analysis of N/D/O-18 stable isotope during ebb and flood tides in summer and autumn in the tidal reach of the Minjiang River. *Acta Sci. Circumstantiae* 42, 314–324 (in Chinese).
- Zhou, Y., Toyoda, R., Suenaga, T., Aoyagi, T., Hori, T., Terada, A., 2022. Low nitrous oxide concentration and spatial microbial community transition across an urban river affected by treated sewage. *Water Res.* 216, 118276.
- Zhu, W., Wang, C., Hill, J., He, Y., Tao, B., Mao, Z., Wu, W., 2018. A missing link in the estuarine nitrogen cycle?: coupled nitrification-denitrification mediated by suspended particulate matter. *Sci. Rep.* 8 (1), 1–10.